Cement and Concrete Research 41 (2011) 579–589

Contents lists available at ScienceDirect

Cement and Concrete Research

journal homepage: http://ees.elsevier.com/CEMCON/default.asp

# Effect of fly ash on the kinetics of Portland cement hydration at different curing temperatures

Mongkhon Narmluk *, Toyoharu Nawa

*Division of Sustainable Resources Engineering, Graduate School of Engineering, Hokkaido University, North13-West8, Kita-ku, Sapporo, 060-8628, Japan*

ARTICLE INFO

*Article history:*
Received 14 July 2010
Accepted 24 February 2011

*Keywords:*
Cement (D)
Fly ash (D)
Hydration (A)
Kinetics (A)
Shrinking-core model

ABSTRACT

This paper describes the effect of fly ash on the hydration kinetics of cement in low water to binder (w/b) fly ash-cement at different curing temperatures. The modified shrinking-core model was used to quantify the kinetic coefficients of the various hydration processes. The results show that the effect of fly ash on the hydration kinetics of cement depends on fly ash replacement ratios and curing temperatures. It was found that, at 20 °C and 35 °C, the fly ash retards the hydration of cement in the early period and accelerates the hydration of cement in the later period. Higher the fly ash replacement ratios lead to stronger effects. However, at 50 °C, the fly ash retards the hydration of the cement at later ages when it is used at high replacement ratios. This is because the pozzolanic reaction of the large volumes of fly ash is strongly accelerated from early in the aging, impeding the hydration of the cement.



## 1. Introduction

Fly ash is widely used as a supplementary cementitious material in high performance concrete because of its benefits in enhancing both fresh and long-term concrete properties and as it promotes eco-friendly construction. Investigations have been carried out mainly to elucidate the pozzolanic reaction of fly ash and its effect on the microstructure of the fly ash-cement paste. Escalante et al. [1] reported that, in paste with water to binder (w/b) ratios of 0.50 and cured in water, fly ash enhanced cement hydration at low temperatures slightly but showed a retarding effect at elevated curing temperatures. Although the effect of fly ash on hydration has been established experimentally, the quantitative influence of fly ash on the kinetics of cement hydration is not well understood. In particular, for modern high-performance concretes with low w/b ratios, the effect of the fly ash on the cement hydration may be different [2]. To predict the performance of fly ash concrete accurately throughout its service life, a more quantitative understanding of the effect of fly ash on cement hydration in low w/b ratio cementitious mixtures is needed.

Kinetic modeling based on the shrinking-core theory can be used to quantify the hydration kinetics of cement. For ordinary Portland cement paste, Park [3,4] and Maruyama [5] have demonstrated the use of this model to simulate the hydration of cement in general and of the different cement components. Results showed good agreement between the model simulations and the experimental data. However, only little experimental data were provided for the verification. Recently, Wang et al. [6–9] has described the application of this model in predicting hydration of fly ash blended cement. Cement hydration and the pozzolanic reaction of fly ash were simulated simultaneously by considering the interaction between the production of calcium hydroxide by cement hydration and its consumption by the pozzolanic reaction of fly ash. This work was able to predict hydration related properties such as chemically bound water, paste porosity, and internal temperature rises, however the development of the degree of hydration of the fly ash containing cement has not been fully elucidated. Only measured hydration data for Portland cement paste obtained from [10] was presented as verification of the model. Termkhajornkit [11] and Saengsoy [12] have pointed out that the degree of hydration of the cement in fly ash-cement paste was higher than that in pure Portland cement paste. This suggests that to simulate the hydration kinetics of the cement in fly ash-cement blends using this model, hydration data for the cement in pure Portland cement paste is not suitable for model calibration. Hydration data for this kind of hydration must be obtained specifically from the blended fly ash-cement paste.

The XRD-Rietveld analysis can be used to monitor cement hydration, but in the case of cement containing fly ash, a part of the cement is replaced by fly ash, and thus the relative amounts of individual cement components are lower. This could increase the relative errors of the XRD-Rietveld analysis of the low-content components such as $C_3A$, and $C_4AF$ [13]. Although there are some studies reported the interactions among the hydration of individual cement components [14,15], these interactions have not been quantitatively established and the mechanisms of these interactions are not well understood. The research to be reported here will first

* Corresponding author. Tel.: +81 11 706 6326; fax: +11 706 7274.
*E-mail address:* mnarmluk@yahoo.com (M. Narmluk).

0008-8846/$ – see front matter © 2011 Elsevier Ltd. All rights reserved.
doi:10.1016/j.cemconres.2011.02.005

focus on the effect of fly ash on the hydration kinetics of the overall cement phase.

The degree of cement hydration and fly ash reactions can be measured separately by using the XRD-Rietveld analysis and the selective dissolution method as described by Termkhajornkit et al. [16]. The shrinking-core model is then used to determine the kinetic parameters of individual hydration processes. These model parameters represent the apparent hydration kinetics of multiple cement components. The results of experiments conducted at three different curing temperatures will be reported.

## 2. Theoretical background

### 2.1. Kinetic model for cement hydration

The shrinking-core model, which was originally developed by Tomosawa [17] and modified in [3–5], is used in this study to simulate the development of cement hydration. This model is expressed as a single equation consisting of three coefficients: $k_d$ the reaction coefficient in the induction period; $D_e$ the effective diffusion coefficient of water through the C–S–H gel; and $k_r$ a coefficient of the reaction rate of cement as shown in Eq. (1) below. These coefficients determine the rate of mass transport through the initial shell layer (a layer of semipermeable, metastable C–S–H product that forms initially when water comes in contact with the cement), the rate of chemical reaction processes, and the rate of diffusion controlled processes. The modeled cement particles are assumed to be spheres surrounded by an initial shell layer. External water diffuses through this layer and reacts with the unhydrated cement at the surface of the core, and then some dissolved ions diffuse outward to the exterior to form new hydration products (C–S–H gel) on the surface of hydrating particles while some take part in forming products locally. Based on this theory, the rate of cement hydration is derived as shown in Eq. (1).

$$\frac{d\alpha}{dt} = \frac{3(S_w/S_0)C_{w-free}}{\left(\nu + w_g\right)\rho_c r_0}\left[\frac{1}{\left(\frac{1}{k_d} - \frac{r_0}{D_e}\right) + \frac{r_0}{D_e}(1-\alpha)^{-1/3} + \frac{1}{k_r}(1-\alpha)^{-2/3}}\right] \quad (1)$$

where $\alpha$ is the degree of cement hydration; $\nu$ is the stoichiometric ratio by mass of water to cement (= 0.23); $w_g$ is the physically bound water in C–S–H gel (= 0.15) [6]; $\rho_c$ is the density of the unhydrated cement; $C_{w-free}$ is the amount of water at the exterior of the C–S–H gel; and $r_0$ is the radius of unhydrated cement particles.

In Eq. (1), the cement particles are assumed to be spherical and of uniform size with an average radius of $r_0 = 3/\left(S\rho_c\right)$ [3,4]. The terms $S$ and $\rho_c$ stand for the Blaine surface area and density of the cement, respectively. As the hydration progresses, the hydration rate decreases with a reduction in the contact area between cement particles and the surrounding water because of the increase in interconnections among cement particles. This effect is accounted for by the term $S_w/S_0$ in Eq. (1) where $S_w$ is the effective surface area of the cement particles in contact with water and $S_0$ is the total surface area if the surface area develops unconstrained [3,4].

The reaction coefficient $k_d$ is assumed to be a function of the degree of hydration as shown in Eq. (2) where $B$ and $C$ are the coefficients determining this factor [3,4]; $B$ controls the rate of the initial shell formation and C controls the rate of the initial shell decay.

$$k_d = \frac{B}{\alpha^{1.5}} + C\alpha^3. \quad (2)$$

In [6–9], the effective diffusion coefficient $D_e$ is assumed to be affected by the tortuosity and pore size of the C–S–H gel and it is expressed in a term for the degree of hydration as shown in Eq. (3). If the C–S–H gel is very porous and has low tortuosity of the pore network, the value of $D_e$ will be high and ions easily diffuse through the gel. The $D_{e0}$ is the initial effective diffusion coefficient of water when C–S–H gel is still only loosely formed at the early period after mixing. With the progress of hydration, the thickness of the C–S–H layer increases, and the diffusivity of water through this layer becomes lower. In [6–9] this effect was expressed by the term $\ln(1/\alpha)$ in Eq. (3) and this term is also included in the model presented here.

$$D_e = D_{e0}\ \ln(1/\alpha). \quad (3)$$

In addition, free water in the capillary pores is depleted as hydration of cement minerals progresses. Some water is bound in the gel pores, and this water is not available for further hydration, an effect that must be taken into consideration in every step of the progress of the hydration [5]. Therefore, the amount of water in the capillary pores $C_{w-free}$ is expressed as a function of the degree of hydration in the previous step as shown in Eq. (4).

$$C_{w-free} = \frac{(W_0 - 0.38 * \alpha * C_0)}{W_0} \quad (4)$$

where $C_0$ and $W_0$ are the mass fractions of cement and water in the mix proportion.

The effect of temperature on these reaction coefficients is assumed to follow Arrhenius's law as shown in Eqs. (5a)–(5d) [3].

$$B = B_{20}\ \exp\left(-\beta_1(1/T - 1/293)\right) \quad (5a)$$

$$C = C_{20}\ \exp\left(-\beta_2(1/T - 1/293)\right) \quad (5b)$$

$$D_e = D_{e20}\ \exp\left(-\beta_3(1/T - 1/293)\right) \quad (5c)$$

$$k_r = k_{r20}\ \exp\left(-(E/R)(1/T - 1/293)\right) \quad (5d)$$

where $\beta_1$, $\beta_2$, $\beta_3$, and $E/R$ are temperature sensitivity coefficients and $B_{20}$, $C_{20}$, $D_{e20}$, and $k_{r20}$ are the values of $B$, C , $D_e$, and $k_r$ at 20 °C.

### 2.2. Working hypothesis of the deposition mechanism

A reduction in $D_e$ is assumed to take place in concert with the increases in the degree of hydration as suggested by Eq. (3). The physical meaning of this phenomenon can be related to the changes in C–S–H gel tortuosity and gel pore diameters [6–9] but no full explanatory mechanism for this has been established.

It was recently reported that at the early stages of aging the inner product is fragile and has low packing density. It later becomes denser and develops into the commonly encountered C–S–H inner product [18]. Further, the work by Bishnoi and Scrivener [19] has proposed that C–S–H is loosely packed in the beginning and that its packing density increase with hydration.

This allows the proposition that the diffusive properties of the C–S–H layer would decrease due to increases in the packing density of the gel as the hydration progresses. The cause of the increase in packing density as considered in the model here is assumed to be due to the deposition of small C–S–H particles/nuclei on the interior pores of the C–S–H layer.

Jennings [20] proposed that C–S–H gel consists of globules which are the smallest basic particles (C–S–H gel particle) with sizes of about 4.2 nm. A C–S–H gel includes two different kinds of gel pores: large and small gel pores. The diameter of the large gel pores range from 3 to 12 nm, and it is possible that some C–S–H particles deposit on the walls of large gel pores, potentially narrowing the diffusion path diameter or completely blocking it, as suggested in Fig. 1.

In this study, it was assumed that the resistance of the C–S–H layers to ion diffusion is due to both the thickness of the C–S–H layers

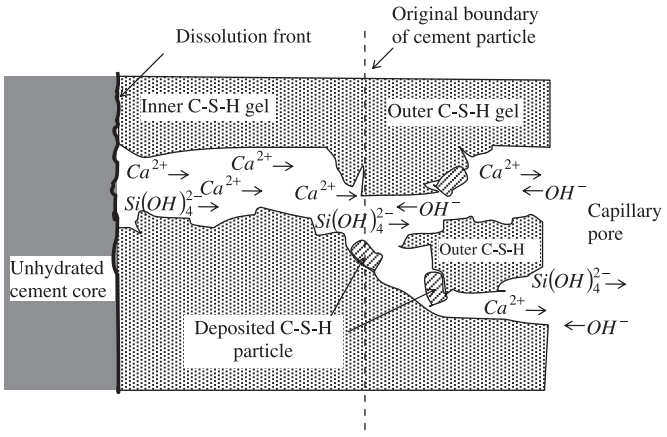


**Fig. 1.** Illustration of the C–S–H particle deposition blocking the pore system.

and the deposition of C–S–H particles in gel pores. At the beginning, C–S–H is loose and porous and contains a range of sizes of small and large gel pores. Deposition of C–S–H particles can occur only in the large gel pores, which can accommodate the C–S–H particles. Ionic diffusion can occur in both small and large gel pores. As a result, when large gel pores are narrowed or blocked, there are small gel pores available for ions to diffuse through. Therefore, it is possible for the deposition of C–S–H particles on the pore walls to occur in parallel with the diffusion of ions through the C–S–H layer. The deposition of C–S–H particles induces more turning and forking (increases tortuosity), resulting in a longer paths for ions to diffuse through the C–S–H layers as the hydration progresses.

### 2.3. Model modifications based on the working hypothesis

When rates of nucleation and growth of nuclei of C–S–H are high, C–S–H particles deposit along the diffusion paths, and such deposition strongly interferes with the ion diffusion. Therefore, the effect of the C–S–H deposition in gel pores on the ionic transport is different at different stages of the nucleation and growth of nuclei of C–S–H as well as it is affected by the amount of already deposited C–S–H.

In modeling of alite and cement hydration, a number of studies have modeled the nucleation and growth of nuclei of hydrates such as C–S–H by the Avrami equation as given in Eq. (6) [21]. Here $F$ is the fraction of the transformed material at time$t$; $k$ is a rate constant; and $m$ is a parameter reflecting the effect of the dimensionality of the growth of the products involved and the nucleus formation mechanism. With Eq. (6), the volume of unreacted substances is given by Eq. (7), where $V_i$ is the unreacted volume at time $t$ [21–22].

$$F = 1 - \exp(-k \cdot t^m) \tag{6}$$

$$V_i = (1-F) = \exp(-k \cdot t^m). \tag{7}$$

Assuming that the kinetics of the deposition of the C–S–H particles/nuclei in the interior gel pores is similar to the kinetics of the nucleation and growth of the hydration product on the exterior surface of the cement particles, a function analogous to the Avrami-type function (Eq. (8)) is proposed to describe the deposition behavior of the C–S–H particles. With this, the fraction of the deposited C–S–H relative to a unit gel porosity is given by Eq. (8).

$$f = 1 - \exp(-k_1 \cdot t^{\kappa}). \tag{8}$$

Further, the volume of the gel pores, which is high at the beginning, is reduced because it becomes increasingly more occupied by deposited C–S–H. Ions can still diffuse through the remaining path ways which however become increasingly more complex (tortuous) and narrower. The volume fraction of the space available for diffusion in the C–S–H gel may be estimated from Eq. (9).

$$1-f = \exp(-k_1 \cdot t^{\kappa}). \tag{9}$$

With Eq. (8), it is suggested that the rate of deposition increases with time. A high rate of deposition of C–S–H particles/nuclei results in lower ionic diffusion rates despite the thickness of the C–S–H layer around the unreacted core. Further, the degree of hydration $\alpha(t)$ at the initial stage, where the rate of hydration is controlled by the rate of nucleation and growth of nuclei, can be represented as [23]:

$$\alpha = k \cdot t^m. \tag{10}$$

Assuming that the effect of deposition of C–S–H particles on the ion diffusion is proportional to the available space for diffusion in the C–S–H gel, from Eqs. (9) and (10), the coefficient of reduction in available space, C, can be expressed by Eq. (11),

$$C = \exp(-\lambda \cdot \alpha^n). \tag{11}$$

Here $n = \kappa/m$ and $\lambda = k_1/k^n$ are kinetic parameters that control the rate and amount of the C–S–H deposition. This study established best values of 4.87 for λ and 5 for $n$.

Finally, the effective diffusion coefficient $D_e$ in Eq. (3) is modified by coefficient C in Eq. (11) giving

$$D_e = D_{e0} \ \ln(1/\alpha) \exp(-\lambda \cdot \alpha^n). \tag{12}$$

In addition, there are significant differences between the inner and the outer C–S–H gel. The inner C–S–H gel has a denser structure and higher density than the outer C–S–H gel and it is commonly assumed that the diffusivity of the gel depends on its porosity or density, as described by Eq. (13).

$$D_e = f(gel.porosity) = g\left(\frac{1}{gel.density}\right). \tag{13}$$

The density is a basic property of the C–S–H gel and its values are more generally available in literatures. Based on Eq. (13), the ratio of the effective diffusion coefficients of the inner and the outer C–S–H gel may be evaluated with the densities, as shown in Eq. (14).

$$\frac{D_e^{out}}{D_e^{inn}} = \frac{\rho_{CSH}^{inn}}{\rho_{CSH}^{out}} \tag{14}$$

where $D_e^{inn}$, $D_e^{out}$ and $\rho_{CSH}^{inn}$, $\rho_{CSH}^{out}$ are the effective diffusion coefficients and densities of the inner and the outer C–S–H gel products, respectively.

Tennis and Jennings [24] reported that the density of the low density C–S–H gel (outer C–S–H gel) is about 1440 kg/m$^3$ and for the high density C–S–H gel (inner C–S–H gel) it is about 1750 kg/m$^3$. With these values, the effective diffusion coefficient of the outer C–S–H gel based on Eq. (14) becomes $D_e^{out} = 1.22 D_e^{inn}$.

A new model equation including the above modifications was derived and the following set of equations is obtained.

$$\frac{d\alpha}{dt} = \frac{3(S_w/S_0)C_{w-free}}{\left(v+w_g\right)\rho_c r_0} \times \left[\frac{1}{\frac{1}{k_d} + \frac{r_0}{D_e^{out}}\left(1-(1+\alpha)^{-1/3}\right) + \frac{r_0}{D_e^{inn}}\left((1-\alpha)^{-1/3}-1\right) + \frac{(1-\alpha)^{-2/3}}{k_r}}\right]. \tag{15}$$

$$D_e^{inn} = D_{e0}^{inn} \ ln(1/\alpha) \ \exp\left(-(\lambda\alpha)^n\right). \tag{16}$$

The pozzolanic reaction between fly ash and calcium hydroxide in cement pastes consumes some amount of water, and to complete the pozzolanic reaction of 1 g of fly ash, the following assumes that 0.1 g of water is bound chemically and that another 0.15 g of water is bound physically as gel water [25]. Therefore, the reduction of the amount of free water at the outer boundary of a hydrating particle must be adjusted by subtracting the amount of water consumed by the pozzolanic reaction of fly ash as suggested in Eq. (17).

$$C_{w-free} = \frac{\left(W_0 - 0.38\alpha C_0 - 0.25\alpha_f F_0\right)}{W_0} \quad (17)$$

where $F_0$ is the mass fraction of the fly ash in the mixed in proportion and $\alpha_f$ is the degree of fly ash hydration obtained experimentally with the selective dissolution method.

## 3. Research methodologies

### 3.1. Materials

Ordinary Portland cement and fly ash which comply with Japanese standard JIS R5210 and JIS A6201 were used in this study. The chemical compositions and physical properties are shown in Table 1 and the mineralogical compositions obtained by the XRD-Rietveld method are given in Table 2.

### 3.2. Mixing procedure

Cement and fly ash powders were mixed at room temperature until homogeneity of the mixture was obtained. Then water including a polycarboxylate-based superplasticizer was added during mixing at low speed for 90 s. After that the paste was further mixed with high speed mixing for 120 s to ensure uniform dispersion of the cementitious particles. After the mixing, the fresh cement paste was cast in cylindrical 5 cm diameter and 10 cm high molds. The molds were carefully sealed to prevent evaporation of water. The mix proportions of the cement pastes are shown in Table 3.

### 3.3. Curing conditions

After the casting process, which took about 30 min for each mix, the paste specimens were cured at 20 °C, 35 °C, or 50 °C.

### 3.4. Method for quantifying the degree of cement hydration

When the required curing ages were reached, the hydration reaction of the cement paste was stopped by crushing the paste specimens into pieces of about 3–5 mm size, and then immersing them in acetone for 24 h. After that the paste sample was dried at 40 °C for 3 h, and next placed in a vacuum desiccator for 2 days. The specimens were then pulverized to be used in powder X-Ray diffraction (XRD) measurements.

The degree of hydration of the cement was measured by the powder XRD equipment, which can quantify the amounts of the crystal phases in the hydrated cement paste. Samples used in the measurements were the hydrated paste powder mixed with 10% of corundum as a reference. The measurement conditions of the XRD were a scanning range of 2θ from 5 to 70° at 40 kV, 20 mA, step width 0.02°, and a scanning speed of 2°/min. The measured XRD data were further analyzed using the Seroquant software which is based on the Rietveld quantitative phase analysis. Final results from this process showed the amounts of unhydrated cement components such as $C_3S$, $C_2S$, $C_3A$, and $C_4AF$, and also $Ca(OH)_2$ as well as the amount of amorphous phases. The overall degree of hydration of the cement can be calculated based on a weighted summation of the degree of hydration of the individual cement components. Further details of the experimental procedures and calculations are provided in [16]. In all cases, non-evaporable water was also determined by the weight loss in an ignition test at 950 °C for 3 h.

### 3.5. Method for quantifying the degree of fly ash hydration

A selective dissolution method was used in quantifying the degree of fly ash hydration. Hydrated fly ash-cement powder was dissolved by an acid solution of 2N HCl at 60 °C for 15 min and subsequently dissolved by a base solution of 5% $NaCO_3$ at 80 °C for 20 min. The accuracy of this method has been verified by [16], which reported the above measurement conditions to give a high accuracy of the degree of fly ash hydration.

### 3.6. Determination of model parameters

The overall degree of cement hydration was determined by the XRD-Rietveld method at various times after mixing the water and cement. By fitting the model simulation with the experimental results, model parameters were systematically determined using commercial software. The effect of the fly ash was then characterized based on

**Table 1**
Chemical composition of the Portland cement and fly ash here and in [12].

| Oxide (%) | This study | | Warangkana's work [12] | |
|---|---|---|---|---|
| | OPC | Fly ash | OPC | Fly ash |
| $SiO_2$ | 21.06 | 59.10 | 21.26 | 68.94 |
| $Al_2O_3$ | 5.77 | 20.20 | 5.28 | 16.44 |
| $Fe_2O_3$ | 2.67 | 8.85 | 2.82 | 3.25 |
| CaO | 63.55 | 3.36 | 64.36 | 1.58 |
| MgO | 1.85 | 1.17 | 2.16 | 1.05 |
| $SO_3$ | 2.28 | 0.12 | 1.97 | 0.18 |
| $TiO_2$ | 0.29 | 1.90 | 0.25 | 0.74 |
| MnO | 0.07 | 0.14 | 0.07 | 0.03 |
| $P_2O_5$ | 0.25 | 2.58 | 0.19 | – |
| $Na_2O$ | 0.26 | 0.34 | 0.25 | 0.23 |
| $K_2O$ | 0.38 | 1.87 | 0.41 | 1.06 |
| Blaine ($cm^2/g$) | 3,400 | 3,740 | 3,520 | 3,970 |
| Density ($g/cm^3$) | 3.16 | 2.33 | 3.17 | 2.15 |
| LOI (%) | 0.614 | 0.960 | 0.56 | 1.25 |

**Table 2**
Mineralogical components of the Portland cement and fly ash in this study and in [12].

| Mineral (%) | This study | | Warangkana's work [12] | |
|---|---|---|---|---|
| | OPC | Fly ash | OPC | Fly ash |
| $C_3S$ | 64.54 | – | 73.03 | – |
| $C_2S$ | 14.04 | – | 10.40 | – |
| $C_3A$ | 4.40 | – | 6.50 | – |
| $C_4AF$ | 9.16 | – | 9.37 | – |
| Gypsum | 0.19 | – | 0.13 | – |
| Mulite | – | 7.09 | – | 2.92 |
| Quartz | – | 8.02 | – | 6.07 |
| Hematite | – | 1.23 | – | 1.67 |
| Amorphous | – | 81.97 | – | 87.57 |

**Table 3**
Mixture proportions of the cement fly ash-cement mixtures used here.

| Mix | w/b (mass fraction) | Fly ash/Cement (vol. fraction) | Superplasticizer[a] (% of binder weight) |
|---|---|---|---|
| OPC | 0.25 | 0/100 | 2.0 |
| | 0.35 | 0/100 | 0.65 |
| FA25 | 0.25 | 25/75 | 1.30 |
| FA50 | 0.25 | 50/50 | 0.65 |

[a] To control the flow diameter of paste at 200 mm.

these parameters. A summary of the input modeling parameters and the output model coefficients are listed in Table 4.

## 4. Results and discussions

### 4.1. XRD-Rietveld results and their validity

This section evaluates the accuracy of the experimental results obtained from the XRD-Rietveld method by comparing the non-evaporable water content (Wn) calculated from the degree of hydration of individual cement components with those obtained from ignition loss measurements. The experimental data for the non-evaporable water and the degree of hydration presented in this paper is an average of the values obtained from three samples, these data show maximum standard deviations below 0.005 for non-evaporable water and below 0.032 for the degree of hydration.

By assuming the amounts of non-evaporable water per gram of the various cement components as 0.234 for $C_3S$, 0.178 for $C_2S$, 0.514 for $C_3A$, and 0.158 for $C_4AF$ [26], the total non-evaporable water content of the hydrated cement can be calculated from the weighted summation of the individual components. The results for the data in this study are plotted in Fig. 2(a)–(b) and show a linear relationship between the Wn values calculated from the Rietveld data and those obtained from the ignition loss. Fig. 3 shows the development of the degree of hydration of the cement in the pastes cured at 20 °C. The degree of cement hydration after 672 h of curing is about 0.65 and 0.80 for pastes with w/b of 0.25 and 0.35, respectively. These values are below the theoretical upper limits calculated from $(w/c)/0.38$ [6,27]. This result confirms that the degree of cement hydration obtained in this study is reliable and that its accuracy is in the acceptable range.

### 4.2. Model evaluation

To evaluate the applicability of our model, a comparison of the degree of cement hydration in OPC paste with a w/b of 0.35 obtained from 1) our model, 2) the Park model, and 3) the experiments is illustrated in Fig. 4. Fig. 4(a) shows the effect of the C–S–H particle deposition on the hydration kinetics. It is clear that our model, which considers the effect of C–S–H particle deposition, exhibits a better agreement with the experimental data than the Park model. The Park model shows overestimated degrees of cement hydration for hydration values above 0.65. From the ideas used in the model modification (Section 2.3 above), the deviations between the results are mainly due to differences in the effective diffusion coefficient. Our model has a lower effective diffusion coefficient at a later age because of the deposition of C–S–H particles blocking the diffusion paths. Fig. 4(b) shows a comparison of the results when our model considers only the effects of differences in effective diffusion coefficients of the inner and the outer C–S–H gel on the cement hydration. As can be seen, there are no differences between the results obtained by our model and the Park model (the continuous and dotted curves overlap, apparently showing only one curve at each temperature). This means that the idea of dividing the C–S–H gel into two zones with different effective diffusion coefficients as in our model did not lead to observable differences in the overall hydration kinetics. This may be ascribed to the small differences in the effective diffusion coefficients (only 22%) and probably also the thinness of the layer of the outer C–S–H gel. Therefore, it can be concluded here that the key mechanism leading to differences between our model and the Park model is the deposition of C–S–H particles blocking the diffusion paths.

**Table 4**
Input modeling parameters and coefficients calculated by the modeling.

| Input parameters | Output coefficients |
|---|---|
| Water to binder ratio, $w/b$ | $B_{20}$ |
| Density of cement, $\rho_c$ | $C_{20}$ |
| Blaine surface area of cement | $D_{e0-20}^{inn}$ |
| Chemical bound water for cement hydration, $\nu = 0.23$ | $k_{r20}$ |
| Physical bound water in hydration product, {w_{g}} = 0.15 | $\beta_1$ |
| Fly ash replacement ratio (0%, 25%, and 50%) | $\beta_2$ |
| Density of fly ash, $\rho_{FA}$ | $\beta_3$ |
| Blaine surface area of fly ash | $E/R$ |
| Degree of pozzolanic reaction of fly ash, $\alpha_f(t)$ | |
| Chemical bound water for pozzolanic reaction = 0.10 | |
| Physical bound water in pozzolanic reaction product = 0.15 | |
| Curing temperatures (20 °C, 35 °C, and 50 °C) | |

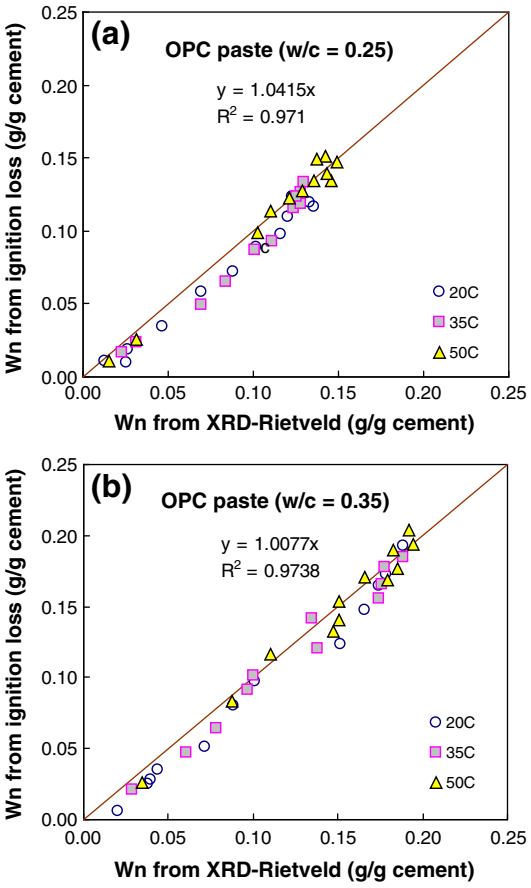


**Fig. 2.** Correlation between non-evaporable water calculated from the degree of hydration and non-evaporable water measured from the ignition loss; (a) w/b = 0.25 and (b) w/b = 0.35.

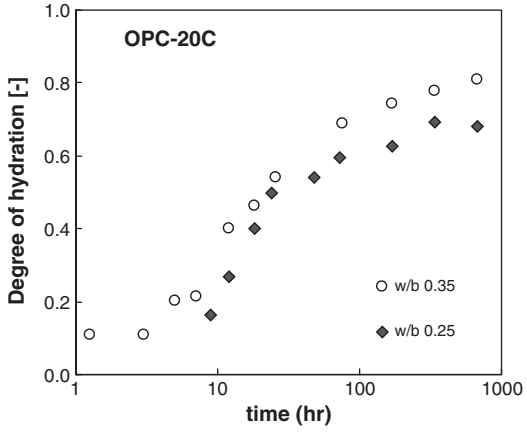


**Fig. 3.** Degree of hydration of OPC pastes cured at 20 °C.

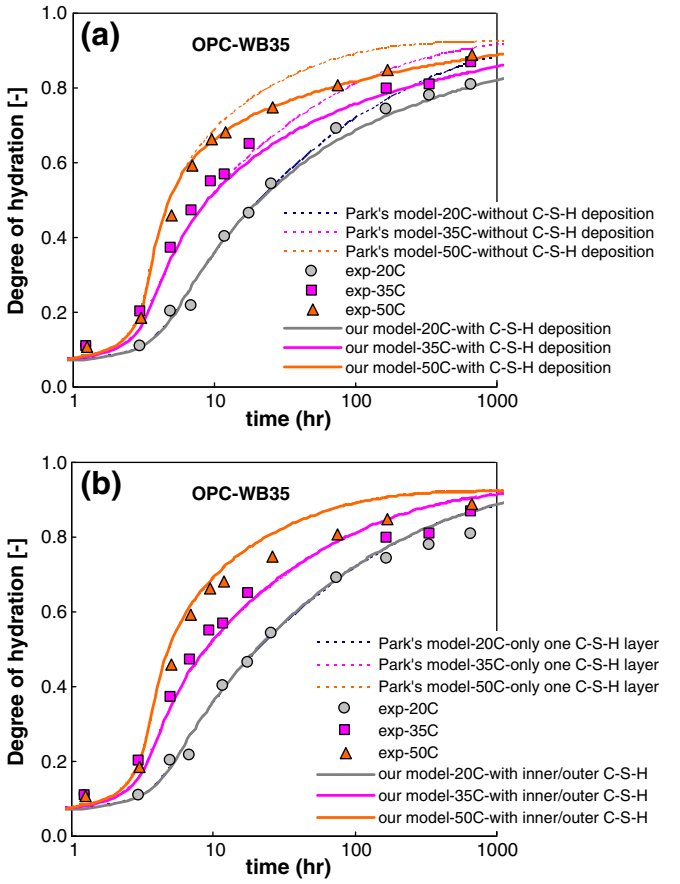


**Fig. 4.** Simulation of the progress of the degree of cement hydration of Portland cement paste with w/b = 0.35, (a) effect of C–S–H particle deposition, (b) effect of differences in effective diffusion coefficients of the inner and the outer C–S–H gel.

### 4.3. Effect of fly ash on the overall hydration kinetics of Portland cement

In this section, our model is used to simulate the experimental results of the cement hydration in fly ash-cement pastes with a w/b of 0.25. The simulated results are presented by curves in Fig. 5(a)–(d). As can be seen, the simulated results are generally in good agreement with the experimental data for all fly ash-cement pastes and all curing temperatures. This demonstrates that our model is valid throughout the period of hydration starting from the onset of the acceleration period to the deceleration period of hydration.

For OPC paste (Fig. 5(a)), the curing temperature shows the acceleration effect on the early hydration rates. The higher curing temperatures lead to faster hydration rates at an early age. However, the degrees of hydration converge to the same level, approximately 0.65, at 1000 h of hydration for all the curing temperatures here. This is consistent with the conclusion of Schindler [28] where there was little or no reduction in the final degree of hydration of Portland cement as a result of curing at different temperatures. Cervera et al. [29] used model simulation to establish that the final degree of hydration of the same sample cured at any temperature only depends on the initial water content of the mixture. This is different from the strength development in which a crossover of strength of pastes cured at different temperatures has been observed [30–32].

For FA25 paste, a similar effect of curing temperature as found in the OPC paste here is also observed, as shown in Fig. 5(b). In this case, the fly ash replacement ratio is about 19.73% by weight of cement. Therefore there is only a moderate effect of fly ash on the overall hydration kinetics of the cement. Overall, the early hydration rates are very similar to those for OPC paste (Fig. 5(a)). For 20 °C curing, the acceleration period of FA25 paste starts at around 10 h which is later than that of the OPC paste. The degree of hydration at 1000 h of all FA25 pastes converges to about 0.75, which is slightly higher than with the OPC pastes.

For FA50 pastes as seen in Fig. 5(c), retardation of the cement hydration at the early period is more pronounced than that found in FA25 pastes. A longer induction period is observed at all curing temperatures. The degree of hydration at 1000 h reaches a level higher than 0.80 for pastes cured at 20 °C and 35 °C. However, for the paste cured at 50 °C, the degree of cement hydration levels off below 0.80 after 100 h of curing. These observed phenomena are related to the effects of fly ash replacement. According to [9] the effect of fly ash on the hydration of the cement includes a dilution effect, an early age physical effect, and a chemical effect.

#### 4.3.1. The dilution effect

It is generally accepted that the final degree of cement hydration increases with the effective w/c ratio [27], and the incorporation of fly ash results in increasing the effective water to cement ratio (w/c). Therefore, the incorporation of fly ash may be seen to enhance the long-term hydration of cement with what has been termed a "dilution" effect [33]. In the results here, this effect can be observed by comparing the final degrees of hydration of the OPC, FA25, and FA50 pastes in Fig. 5(a)–(c). Here the degree of hydration of the cement late in the curing period increases with the fly ash replacement ratio, regardless of curing temperature. To show this more clearly, the hydration kinetics of the cement in pastes containing different replacement ratios of fly ash at 20 °C are compared in Fig. 5(d). The figure shows a clear increase in the long-term degree of hydration with higher replacement ratios of fly ash, especially at the high fly ash replacement condition (FA50).

#### 4.3.2. The physical effect

The effect of fly ash replacement is also related to the physical properties of fine fly ash particles. There are two kinds of physical effects of fly ash on cement hydration: early retardation of hydration and an increase in available nucleation sites. The early slowing down of hydration in the presence of fly ash been reported by numerous papers [34–38]. This is related to the condition of the fly ash surface. Calcium ions adsorb on the fly ash surface, thus lowering the $[Ca^{2+}]$ in the bulk solution. It is may be that the reduction of $[Ca^{2+}]$ could lead to a lower Ca/Si ratio in the solution and also in the initial shell of the fly ash-cement pastes. Gartner et al. [23] and Gartner and Jennings [39] have shown that the degree of instability of the metastable C–S–H layer (termed the initial shell in this paper) is related to its Ca/Si ratio, and that lower Ca/Si ratios lead to less instability of the C–S–H layer. Garrault and Nonat [40] and Bullard and Flatt [41], in studies on $C_3S$ hydration in dilute solution (liquid/solid = 50), pointed out that nucleation and growth of C–S–H nuclei at the initial period are faster at low lime ($Ca(OH)_2$) concentrations. It is difficult to extrapolate these findings to explain the hydration kinetics of the fly ash-cement pastes presented here. This is due to the differences in the liquid/solid ratios and the presence of the surface of fly ash. Generally, the $[Ca^{2+}]$ in solutions of fly ash-cement pastes is lower than that in OPC paste; but the findings in [40] cannot explain the hydration phenomena in fly ash-cement pastes.

However, it could be hypothesized that the initial shell with a lower Ca/Si ratio in fly ash-cement pastes would transform to a more stable C–S–H at a slower rate than that with higher the Ca/Si ratio in OPC paste. This could partly explain the extended induction period of hydration in fly ash-OPC paste. The retardation effect, early slowing down, is compensated by a physical acceleration effect in that the fly ash surface provides additional nucleation sites for hydration products to precipitate on [9]. This is indicated in Fig. 5(d) where the cement hydration in fly ash-cement paste shows a longer induction period and a higher hydration rate thereafter for the fly ash containing samples.

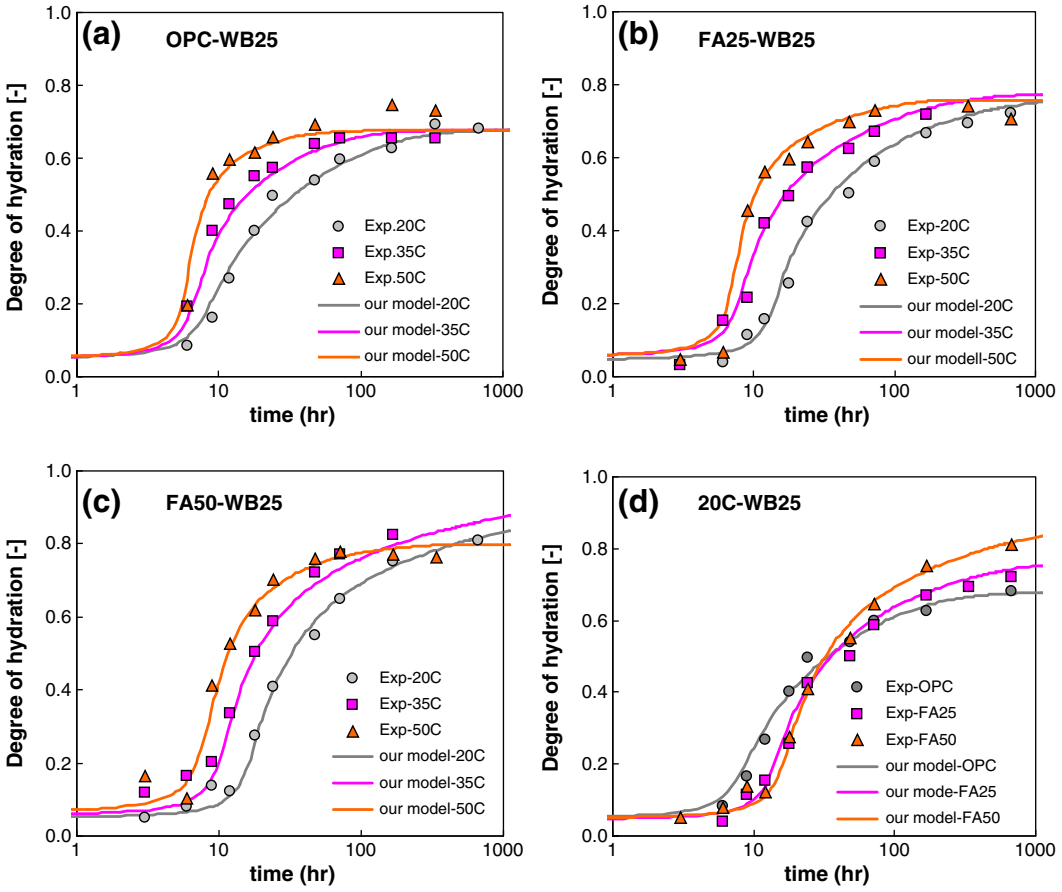


**Fig. 5.** Simulation of the progress of the degree of cement hydration of fly ash-cement paste with w/b = 0.25: (a) OPC paste, (b) FA25 paste, (c) FA50 paste, (d) different fly ash-cement pastes at 20 °C.

*4.3.3. The chemical effect*

Fly ash is chemically involved in the cement hydration in two ways. First, cement produces $Ca(OH)_2$ in the hydration while fly ash consumes $Ca(OH)_2$ in the pozzolanic reaction. Second, both cement and fly ash consume water in their hydration reactions [9]. The first effect results in a lower $Ca(OH)_2$ concentration that would contribute to an acceleration of $Ca^{2+}$ dissolution from the cement particles. With the second effect, and for high fly ash replacement ratios the pozzolanic reaction of the large volume of fly ash could significantly contribute to increases in water consumption, even when fly ash needs much less water for its reaction than cement, and the water consumed here could consequently hamper the cement hydration. It has been reported that the complete reaction 1 ml of fly ash produces 2.52 ml and 3.25 ml net volumes of hydration products for 25% and 50% replacement ratios of fly ash, by volume of binder [2]. The marked difference between the volumes of the unhydrated cement and the volumes of the hydration products strongly contributes to filling the capillary space.

All of the above mentioned effects may not be clearly observable at low curing temperatures when the pozzolanic reaction of fly ash is slow. However, at higher curing temperatures these effects may become observable. As in the case of FA50 cured at 50 °C in Fig. 5(c), the degree of hydration of the cement at the later curing stage is lower than when cured at 20 °C and 35 °C. This slowing down at high curing temperature is supported by the reaction kinetics of fly ash in Fig. 6. Fig. 6(a) and (b) shows the development of the pozzolanic reaction of fly ash in FA25 and FA50 pastes at different curing temperatures. The results for both mixtures show that at 50 °C the pozzolanic reaction of fly ash starts with a high rate of increase as early as 12 h after mixing, while at 35 °C and 20 °C the high rate of increase starts after 72 h and 336 h, respectively. The early high pozzolanic reaction of fly ash in FA50 paste at 50 °C confirms that the contribution of fly ash in consuming water and producing C–S–H to fill the capillary pores is the main factor that impedes the hydration of the cement phase.

From the results reported here, the effect of the curing temperature on cement hydration as reported by Schindler [28] and Cervera et al. [29] may not be valid when the cement does not hydrate without additives like fly ash. The results here further show that the effect of fly ash on hydration of the cement depends on the fly ash replacement ratio and the timing of the onset of the pozzolanic reaction, not on the extent of pozzolanic reaction. Also, the results suggest that, in low w/b pastes containing high replacement volumes of fly ash and subjected to curing at high temperatures, the hydration of the cement is more likely to become retarded because of insufficient water and/or insufficient space for the C–S–H gel from the cement hydration is able to grow.

*4.4. Effect of fly ash on the reaction coefficients of hydration in different processes*

Model coefficients determined by the best-fit analysis are given in Table 5. It can be seen that $B_{20}$ and $k_{r20}$ are constant for all mixtures. This suggests that the rate of formation of the initial shell in the induction period and the rate of chemical reaction are independent of the incorporation of the fly ash admixture and water to binder ratio. The $C_{20}$ and $D_{e0-20}^{inn}$ reaction coefficients vary with the fly ash replacement ratio and/or w/b ratio, and the effect of fly ash on cement hydration discussed in this section is focused on the change in $C_{20}$ rather than $k_d$ (for the early period) and $D_{e0-20}^{inn}$ (for the later period). It must be kept in mind that the coefficient $C_{20}$ controls the rate of decay of the initial shell (a semipermeable, metastable C–S–H layer). The growth of the more stable C–S–H nuclei, indicated by the onset of the acceleration period, is

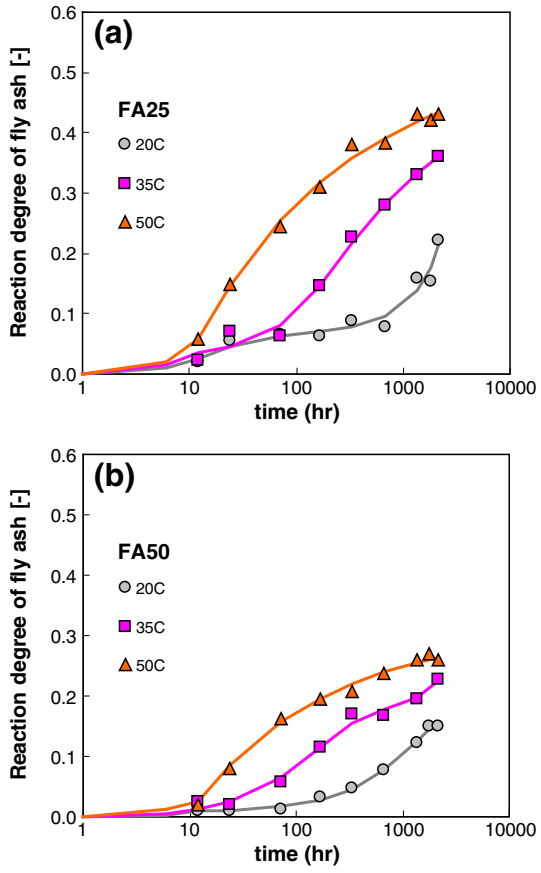


**Fig. 6.** Progress of the degree of pozzolanic reaction of fly ash at three curing temperatures (20 °C, 35 °C, and 50 °C): (a) FA25 paste, (b) FA50 paste.

associated with a conversion of this metastable layer [42]. A decrease in $C_{20}$ suggests that the rate of decay of the initial shell becomes slower, resulting in a delay of the onset of the acceleration period. In this study, the value of $C_{20}$ could be influenced by two factors: the presence of superplasticizer and the presence of fly ash, and this will be discussed next.

In Portland cement paste without fly ash replacement, an increase in the w/c ratio has a limited effect the hydration kinetics before the acceleration period [43], therefore the change in $C_{20}$ observed in the results reported here can be attributed to the presence of the superplasticizer. It is generally accepted that the addition of a superplasticizer delays the onset of the acceleration period [44]. Molecules of superplasticizer hinder water and $Ca^{2+}$ ion diffusion across the solution-cement interface. Also, $Ca^{2+}$ ions form complexes with the superplasticizer molecules, inhibiting the nucleation and growth of Ca-rich species [45]. Therefore addition of superplasticizer delays the acceleration of hydration, in other words it retards the rate of decay of the initial shell layer. The effect of the superplasticizer can be seen by comparing the two OPC pastes of different w/b ratios in Table 5. The value of $C_{20}$ of the OPC paste with w/b = 0.25 is lower than that of the paste with w/b = 0.35. This suggests that the onset of acceleration period would start at a later time, as also shown in Fig. 3.

For fly ash-cement pastes, the delay of the onset of the acceleration period is due to a combined effect of the superplasticizer and the fly ash contents. For example, at w/b = 0.25 the FA50 paste contains much less superplasticizer than the OPC paste and as a result its acceleration period would start earlier. However, a smaller $C_{20}$ value and a longer induction period are observed as shown in Table 5, Fig. 7, and Fig. 5(d). The effect of fly ash on the reduction of $C_{20}$ can be explained by adsorption of $Ca^{2+}$ on the fly ash surface as described in the previous section. In addition, the fly ash could supply significant amounts of silicate ions to the solution since the early age [41]. This effect also leads to a lower Ca/Si ratio of the solution and in the initial shell of fly ash-cement pastes [23,39], and results in a longer induction period for the hydration in fly ash-OPC pastes. The results suggest that the retardation effect due to adsorption of $Ca^{2+}$ on the fly ash surface and/or additional supplies of silicate ions is stronger than that caused by the addition of superplasticizer.

Fig. 7 shows that the initial effective diffusion coefficient $D^{inn}_{e0-20}$ increases with the fly ash replacement volume. Especially, when the fly ash content increases from 25% to 50% by volume, the $D^{inn}_{e0-20}$ increases considerably. This indicates that fly ash influences the diffusion process of the cement hydration. This could be explained by the silica-rich characteristics of fly ash. Dissolved silica ions $Si(OH)_4^{2-}$ from the fly ash could diffuse into the cement particles [34]. The fly ash would then serve as an additional silica source for hydration product formation, thus lowering the Ca/Si molar ratio of the overall C–S–H product including the C–S–H around cement grains. This could eventually lead to a higher effective diffusivity of water into the C–S–H gel. The average Ca/Si molar ratio of the overall C–S–H gel in fly ash-cement pastes, calculated by the mass balance method [46,47], is plotted as a function of the fly ash replacement ratio in Fig. 8. It is clear that, with 28 days of hydration time, the average Ca/Si molar ratio measured in the present study decreases linearly from 2.1 for OPC paste to 1.55 for FA50 paste which agrees with data in the literature [47–51]. Although there are differences in the absolute Ca/Si values among the data reported in Fig. 8, because of the differences in material compositions and age of test pieces, the tendency towards lowerings of the Ca/Si molar ratio is similar. Wang et al. [49] and Escalante and Sharp [50] reported very similar slopes of Ca/Si reductions specifically for C–S–H gel around cement particles. Sagawa et al. [52] reported that the density of the C–S–H gel in blast furnace slag-cement paste increases with the Ca/Si ratio, and decreases with increasing H/Si ratios (H = $H_2O$). Suda et al. [53]

**Table 5**
Model coefficients of Eqs. (5a)–(5d) obtained from the regression analysis.

| w/b | % Fly ash | $B_{20}$ ($\times 10^{-9}$) | $C_{20}$ ($\times 10^{-2}$) | $D^{inn}_{e0-20}$ [b] ($\times 10^{-8}$) | $k_{r20}$ ($\times 10^{-4}$) | $\beta_1$ | $\beta_2$ | $\beta_3$ | $E/R$ |
|---|---|---|---|---|---|---|---|---|---|
| 0.25 | 0 | 1 | 3.81 | 4.62 | 1.52 | 10 | 900 | 6000 | 6173 |
| | 25 | 1 | 2.79 | 5.10 | 1.52 | 10 | 900 | 4500 | 5075 |
| | 50 | 1 | 2.18 | 7.55 | 1.52 | 10 | 900 | 4300 | 3022 |
| 0.35 | 0 | 1 | 4.83 | 4.62 | 1.52 | 10 | 900 | 6000 | 6173 |

[b] $D^{inn}_{e0-20}$ is the initial effective diffusion coefficient of the inner C–S–H gel at 20 °C.

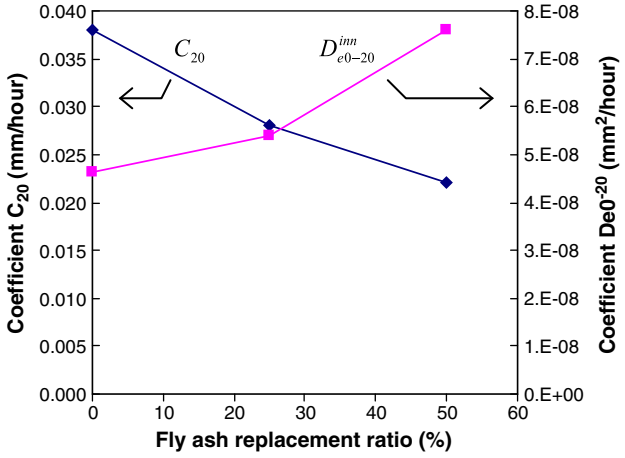


**Fig. 7.** Effect of the fly ash replacement ratio on the reaction coefficient $C_{20}$ (left, blue) and the effective diffusion coefficient $D^{inn}_{e0-20}$ (right, purple).

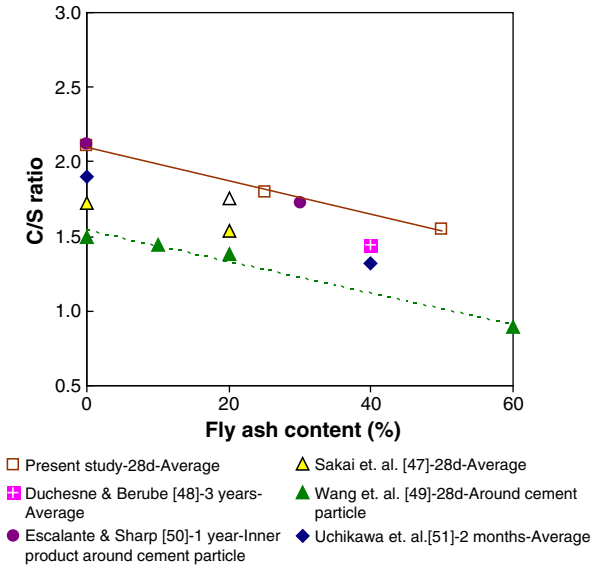


**Fig. 8.** Effect of the fly ash replacement ratio on the Ca/Si molar ratio of C–S–H gel.

also reported that the average density of the C–S–H gel from various cementitious materials increased linearly with the Ca/Si molar ratios. This relationship can be described as $\rho_{CSH} = 0.241 \cdot (Ca/Si) + 1.72\,(g/cm^3)$. In fact, a higher density of the C–S–H gel is associated with a greater packing density of the C–S–H particles. Therefore, the lower Ca/Si molar ratio of the C–S–H gel of paste containing fly ash can be interpreted to be a cause of the lower packing density and the higher diffusivity of the C–S–H gel.

### 4.5. Effect of fly ash on temperature sensitivity coefficients

The temperature sensitivity of individual hydration processes can be considered via the coefficients $\beta_1$, $\beta_2$, $\beta_3$, and $E/R$ listed in Table 5. These coefficients were determined from hydration data of the cement phase obtained at three different curing temperatures. The results show that the temperature sensitivity factors ($\beta_1$ and $\beta_2$) for the formation and the decay of the initial shell are the same for all pastes. For neat OPC pastes with different w/c ratios, it has been found that the temperature sensitivity factor for the diffusion process ($\beta_3$) is unchanged. This result has also been reported in Park et al. [3]. In these three lines, we are talking about the values of beta in the first and the last rows of Table 5. It is not related to the effect of fly ash in Fig. 9.

The data also suggests that the chemical reaction and diffusion processes are most sensitive to changes in curing temperatures, as represented by $E/R$ and $\beta_3$, respectively. The degree of temperature sensitivity of the process of formation and decay of the initial shell represented by $\beta_1$ and $\beta_2$ are much lower than the chemical reaction and diffusion processes. The low $\beta_1$ and $\beta_2$ values suggest that the rates of cement hydration in the induction period of pastes cured at different temperatures are similar. The detailed reasons for this similarity are not established.

Incorporation of fly ash in the cement paste clearly reduces the $E/R$ and $\beta_3$ values, as shown in Fig. 8. This suggests that the chemically controlled and the diffusion controlled processes of cement hydration are less sensitive to changes in temperature when fly ash is added. Related to this, Ma et al. [54] also reported that $E/R$ reduced from 4690 J/K for pure Portland cement paste to 3210 J/K for Portland cement paste containing 17% of low-calcium fly ash. Based on available information from the literature, the mechanism of this phenomenon is still not clearly elucidated. To fully and satisfactorily explain the mechanism, more detailed investigation is necessary.

### 4.6. Applicability of the model to other fly ash-cement mixtures

To verify our model with other fly ash-cement mixtures, both the degree of cement hydration and the degree of pozzolanic reaction of fly ash are needed. However, there is very little data in the literature that reports both the kinetics of hydration and the pozzolanic reaction together. One report however, Warangkana et al. [12], provides both kinds of data, quantitatively, and from here the data there will be used to discuss the applicability of our model in the paper.

In [12], the degree of hydration and pozzolanic reaction in cement pastes with fly ash replacement ratios of 0%, 25%, and 50% (by volume) were studied at a water to binder ratio of 1:1 by volume fraction (approximately 0.31 by weight). Curing conditions were varied and only the case of sealed curing at 20 °C is used in the simulations detailed here. The chemical and physical properties of cement and fly ash used in [12] are given in Tables 1 and 2.

Since the hydration data for early curing ages is not provided in [12], it is assumed here that the fly ash in [12] would display similar influences on the early age hydration of the cement as those established in our study. Therefore, the model coefficients $B_{20}$ and $C_{20}$ obtained earlier for this study were applied to [12]. Only the $D_{e0-20}^{inn}$ and $k_{r20}$ were determined from fitting the model to the experimental data.

Based on the above and with the material properties of [12], the hydration kinetics of cement was simulated by our model, and the results of the simulation are shown with curves in Fig. 10. It can be seen

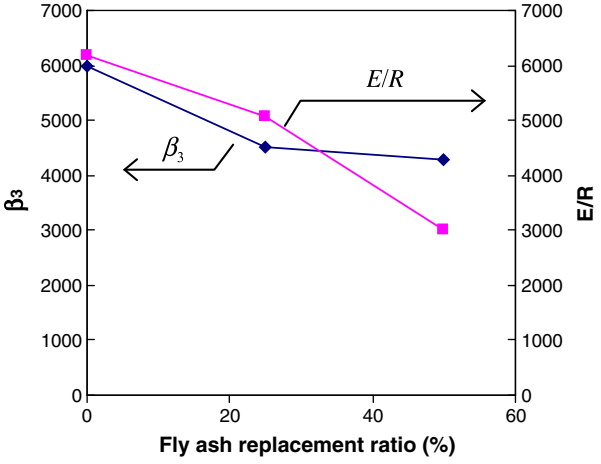


**Fig. 9.** Effect of the fly ash replacement ratio on the temperature sensitivity of the diffusion process $\beta_3$ (left, blue) and of the chemical reaction $E/R$ (right, purple).

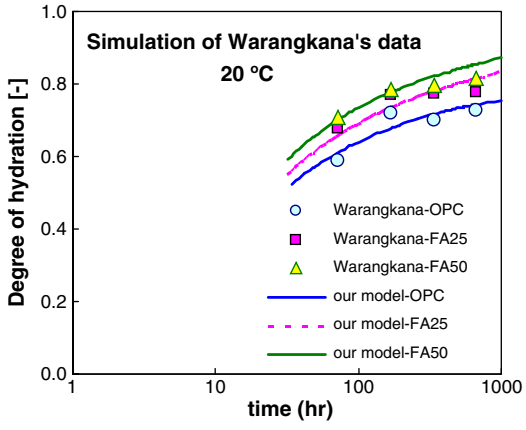


**Fig. 10.** Simulation of the progress of the degree of cement hydration in Warangkana's work [12].

**Table 6**
Model coefficients for fly ash-cement paste in Warangkana's work [12].

| w/b | % Fly ash | $D_{e0-20}^{inn}$ ($\times 10^{-8}$) | $k_{r20}$ ($\times 10^{-4}$) |
|---|---|---|---|
| 0.31 | 0 | 4.32 | 1.67 |
| | 25 | 4.84 | 1.67 |
| | 50 | 5.21 | 1.67 |

that the model developed here is in reasonably good agreement with the [12] experimental data for OPC paste but slightly overestimates the hydration of cement in the fly ash-cement mixtures at later aging times. Table 6 indicates that $k_{r20}$ is not changed and $D_{e0-20}^{inn}$ increases with the fly ash replacement ratio. This is consistent with the findings with the cement and fly ash that we report. However, the increment in the $D_{e0-20}^{inn}$ values in [12] at the same fly ash replacement ratios is lower than the results with the fly ash in this investigation. Sakai et al. [47] reported that the amorphous content affects the pozzolanic reaction of the fly ashes at later ages. A higher amorphous content leads to a greater degree of pozzolanic reaction of the fly ash, and this effect is reduced when the fly ash replacement ratio increases. It may be expected that the fly ash with a higher amorphous content is more effective in enhancing the $D_{e0-20}^{inn}$ of C–S–H gel than that with low amorphous content. However, the results reported here show that the fly ash in [12] which has slightly higher amorphous content is less effective in enhancing the $D_{e0-20}^{inn}$ of the C–S–H gel, as shown in Table 6. This indicates that the diffusive properties of C–S–H around cement grains may be controlled by the chemical properties of the cement.

Park et al. [3] reported that cement with a higher $C_3S$ content have a lower $D_{e0-20}^{inn}$. The OPC used in [12] contains much more $C_3S$ than the OPC used in this study, as shown in Table 2. Considering this, it may be that the of the C–S–H around the cement particles is primarily controlled by the chemical composition of the cement grains, and that it is modified when fly ash is added. Therefore, in modeling the $D_{e0-20}^{inn}$ with other fly ash-cement mixtures, the $C_3S$ content in the cement and the amorphous content in the fly ash are important factors.

Besides, the kinetics of cement hydration can be affected by the minor components of the cement. Rahhal et al. [55] found that a high content of sulfate in the form of gypsum slowed down the rates of hydration of cements and lengthened the induction period if the cement had a low $C_3A$ content. Schindler and Folliard [56] have also shown that the induction period of the hydration tended to become extended when the sulfate content increased. The rate of hydration in the acceleration period increased considerably with sulfate content. These are consistent with Brown et al. [57] who previously reported that the presence of calcium sulfate ($CaSO_4$) in solution slightly retards hydration of pure $C_3S$ at the early age but accelerates it thereafter. This suggests that to apply our model to fly ash-cement mixtures with different sulfate contents it may be necessary to adjust the model coefficients $B$ and $C$ in Eq. (2) which express the hydration rate in the induction and acceleration periods. However, at present, the mechanisms for the effect of sulfate on the hydration of the cement have not been well established. It would be premature to consider including the effect of sulfate in the model.

In summary, the model can be used to simulate the hydration kinetics in a fly ash-paste mixture with fairly good accuracy by using the same expression of effective diffusion coefficients as in Eq. (11). The results show that fly ash has some influence on the diffusive properties of C–S–H around cement grains. Regardless of the chemical composition of the cement and fly ash, higher fly ash replacement ratios give rise to increases in the diffusive properties of the C–S–H around cement grains. The magnitude of increase in the diffusive properties of C–S–H due to fly ash replacement appears to be governed by the chemical composition of the cement grains, presumably the $C_3S$ content.

## 5. Conclusions

In this paper, the effect of fly ash on the hydration kinetics of Portland cement in fly ash-Portland cement mixtures of low w/b ratios was studied at three curing temperatures. The shrinking-core model was used in a modified form in quantifying the kinetics parameters of the cement hydration. Based on the results, the following conclusions may be drawn.

5.1 With the concept of densification of C–S–H gel due to deposition of C–S–H particles in gel pores, the model can better simulate the hydration kinetics of cement in the later hydration period than the Park model.

5.2 The effect of fly ash on the hydration of cement is dependent on the curing temperature and the fly ash replacement ratio. At commonly encountered curing temperatures (not higher than 35 °C), the presence of fly ash at all replacement ratios accelerates hydration of cement due to the cement dilution effect. However, at higher curing temperatures (50 °C) and high fly ash replacement ratios, the pozzolanic reaction of fly ash becomes important because it competes with the cement hydration in consuming water and producing large amounts of reaction product from early ages, and this may counteract the dilution effect. As a result, hydration is impeded.

5.3 When fly ash is incorporated, the effective diffusion coefficient of C–S–H around cement particles increases. This facilitates water diffusion through the C–S–H layer, and consequently contributes to an acceleration of the cement hydration at later aging times.

## Acknowledgment

We wish to thank The Hitachi Scholarship Foundation for the financial support for the Ph.D. study of the first author.

## References

[1] J.I. Escalante-Garcia, J.H. Sharp, Effect of temperature on the hydration of the main clinker phases in Portland cements: part II, Blended cements, Cem. Concr. Res. 28 (1998) 1259–1274.
[2] L. Lam, Y.L. Wong, C.S. Poon, Degree of hydration and gel/space ratio of high volume fly as/cement system, Cem. Concr. Res. 30 (2000) 747–756.
[3] K.B. Park, T. Noguchi, J. Plawsky, Modeling of hydration reactions using neural networks to predict the average properties of cement paste, Cem. Concr. Res. 35 (2005) 1676–1684.
[4] K.B. Park, N.Y. Jee, I.S. Yoon, H.S. Lee, Prediction of temperature distribution in high-strength concrete using hydration model, ACI Mater. J. 105 (2008) 180–186.
[5] I. Maruyama, T. Matsushita, T. Noguchi, Numerical modeling of Portland cement hydration based on particle kinetic model and multi-component concept, Proceedings of the 12th International congress of chemistry of cement, Montreal, 2007.
[6] Xiao-Yong Wang, Han-Seung Lee, Ki-Bong Park, Simulation of low-calcium fly ash blended cement hydration, ACI Mater. J. 106 (2009) 167–175.
[7] Xiao-Yong Wang, Han-Seung Lee, A model for predicting the carbonation depth of concrete containing low-calcium fly ash, Constr. Build. Mater. 23 (2009) 725–733.
[8] Xiao-Yong Wang, Han-Seung Lee, Modeling the hydration of concrete incorporating fly ash or slag, Cem. Concr. Res. 40 (2010) 984–996.
[9] Xiao-Yong Wang, Han-Seung Lee, Simulation of a temperature rise in concrete incorporating fly ash or slag, Mater. Struct. 43 (2009) 737–754.
[10] T. Matsushita, S. Hoshino, I. Maruyama, T. Noguchi, K. Yamada, Effect of curing temperature and water to cement ratio on hydration of cement compounds, Proceedings of the 12th International Congress of Chemistry of Cement, Montreal, 2007.
[11] P. Termkhajornkit, T. Nawa, K. Kurumisawa, Effect of water curing conditions on the hydration degree and compressive strengths of fly ash-cement paste, Cem. Concr. Compos. 28 (2006) 781–789.
[12] W. Saengsoy, T. Nawa, P. Termkhajornkit, Influence of relative humidity on compressive strength of fly ash cement paste, J. Struct. Constr. Eng. 73 (2008) 1433–1441.
[13] A.G. De la Torre, M.A.G. Aranda, Accuracy in Rietveld quantitative phase analysis of Portland cements, J. Appl. Crystallogr. 36 (2003) 1169–1176.
[14] I. Odlera, J. Schüppstuhla, Combined hydration of tricalcium silicate and β-dicalcium silicate, Cem. Concr. Res. 12 (1982) 13–20.
[15] C. Plowman, J.G. Cabrera, Mechanism and kinetics of hydration of C3A and C4AF Extracted from cement, Cem. Concr. Res. 14 (1984) 238–248.

[16] P. Termkhajornkit, T. Nawa, M. Nakai, T. Saito, Effect of fly ash on autogenous shrinkage, Cem. Concr. Res. 36 (2005) 473–482.
[17] F. Tomosawa, A hydration model of cement, Proc. of Annual Meeting on Cement Technology, Cement Association of Japan, 28, 1974, pp. 53–57, (in Japanesse).
[18] E. Gallucci, P. Mathur, K. Scrivener, Microstructural development of early age hydration shells around cement grains, Cem. Concr. Res. 40 (2010) 4–13.
[19] Shashank Bishnoi, Karen L. Scrivener, Studying nucleation and growth kinetics of alite hydration using μic, Cem. Concr. Res. 39 (2009) 849–860.
[20] H.M. Jennings, Refinements to colloid model of C–S–H in cement: CM-II, Cem. Concr. Res. 38 (2008) 275–289.
[21] Jie Zhang, Emily A. Weissinger, Sulapha Peethamparan, George W. Scherer, Early hydration and setting of oil well cement, Cem. Concr. Res. 40 (2010) 1023–1033.
[22] Richard A. Livingston, Fractal nucleation and growth model for the hydration of tricalcium silicate, Cem. Concr. Res. 30 (2000) 1853–1860.
[23] E.M. Gartner, J.F. Young, D.A. Damidot, I. Jawed, Hydration of Portland Cement, Structure and Performance of Cement, 2nd ed. Spon Press, London, 2002.
[24] P.D. Tennis, H.M. Jennings, A model for two types of calcium silicate hydrate in the microstructure of Portland cement pastes, Cem. Concr. Res. 30 (2000) 855–863.
[25] K. Maekawa, R. Chaube, T. Kishi, Modeling of Concrete Performance: Hydration, Microstructure Formation and Mass Transport, E & FN SPON, London, 1998.
[26] K. van Breugel, *Simulation of hydration and formation of structure in hardening cement-based materials*, PhD thesis, TU Delft, The Netherland, 1991.
[27] H.F.W. Taylor, Cement Chemistry, Academic Press, London, 1990.
[28] A. Schindler, Effect of temperature on hydration of cementitious materials, ACI Mater. J. 101 (2004) 72–81.
[29] M. Cervera, J. Oliver, T. Prato, Thermo-chemo-mechanical model for concrete I: hydration and aging, J. Eng. Mech. 125 (1999) 1018–1027.
[30] K.O. Kjellsen, R.J. Detwiler, O.E. Gjorv, Development of microstructures in plain cement pastes hydrated at different temperatures, Cem. Concr. Res. 21 (1991) 179–189.
[31] Y. Maltais, J. Marchand, Influence of curing temperature on cement hydration and mechanical strength development of fly ash mortars, Cem. Concr. Res. 27 (1997) 1009–1020.
[32] J.I. Escalante-Garcia, J.H. Sharp, The microstructure and mechanical properties of blended cements hydrated at various temperatures, Cem. Concr. Res. 31 (2001) 695–702.
[33] Philippe Lawrence, Martin Cyr, Erick Ringot, Mineral admixtures in mortars: effect of inert materials on short-term hydration, Cem. Concr. Res. 33 (2003) 1939–1947.
[34] K. Ogawa, H. Uchikawa, K. Takemoto, I. Yasui, The mechanism of the hydration in the system $C_3S$-pozzolana, Cem. Concr. Res. 10 (1980) 683–696.
[35] W. Fajun, M.W. Grutzeck, D.M. Roy, The retarding effects of fly ash upon the hydration of cement pastes: the first 24 hours, Cem. Concr. Res. 15 (1985) 174–184.
[36] B.W. Langan, K. Weng, M.A. Ward, Effect of silica fume and fly ash on heat of hydration of Portland cement, Cem. Concr. Res. 32 (2002) 1045–1051.
[37] W. Nocun-Wczelik, Heat evolution in hydrated cementitious systems admixtured with fly ash, J. Therm. Anal. Calorim. 65 (2001) 613–619.
[38] V. Rahhal, R. Talero, Influence of two different fly ashes on the hydration of Portland cements, J. Therm. Anal. Calorim. 78 (2004) 191–205.
[39] E.M. Gartner, H.M. Jennings, Thermodynamics of calcium silicate hydrates and their solutions, J. Am. Ceram. Soc. 70 (1987) 743–749.
[40] S. Garrault, A. Nonat, Hydrated layer formation on tricalcium and dicalcium silicate surfaces: experimental study and numerical simulations, Langmuir 17 (2001) 8131–8138.
[41] J.W. Bullard, R.J. Flatt, New insights in to the effect of calcium hydroxide precipitation on the kinetics of tricalcium silicate hydration, J. Am. Ceram. Soc. 93 (2010) 1894–1903.
[42] J.W. Bullard, H.M. Jennings, R.A. Livingston, A. Nonat, G.W. Scherer, J.S. Schweitzer, K.L. Scrivener, J.J. Thomas, Mechanisms of cement hydration, Cem. Concr. Res. (2010), doi:10.1016/j.cemconres.2010.09.011.
[43] R. Berliner, M. Popovici, K.W. Herwig, M. Berliner, H.M. Jennings, J.J. Thomas, Quasielastic neutron scattering study of the effect of water-to-cement ratio on the hydration kinetics of tricalcium silicate, Cem. Concr. Res. 28 (1998) 231–243.
[44] F. Puertas, H. Santos, M. Palacios, S. Martínez-Ramírez, Polycarboxylate superplasticiser admixtures: effect on hydration, microstructure and rheological behaviour in cement pastes, Adv. Cem. Res. 17 (2005) 77–89.
[45] M.Y.A. Mollah, W.J. Adams, R. Schennach, D.L. Cocke, A review of cement—superplasticizer interactions and their models, Adv. Cem. Res. 12 (2000) 153–161.
[46] Zhao-Qi Wu, J.F. Young, The hydration of tricalcium silicate in the presence of colloidal silica, J. Mater. Sci. 19 (1984) 3477–3486.
[47] E. Sakai, S. Miyahara, S. Ohsawa, S.H. Lee, M. Daimon, Hydration of fly ash cement, Cem. Concr. Res. 35 (2005) 1135–1140.
[48] J. Duchesne, M.A. Berube, Effect of supplementary cementing materials on the composition of cement hydration products, Adv. Cem. Based Mater. 2 (1995) 43–52.
[49] A. Wang, C. Zhang, W. Suna, Fly ash effects: II. The active effect of fly ash, Cem. Concr. Res. 34 (2004) 2057–2060.
[50] J.I. Escalante-Garcia, J.H. Sharp, The chemical composition and microstructure of hydration products in blended cements, Cem. Concr. Compos. 26 (2004) 967–976.
[51] H. Uchikawa, S. Uchida, K. Ogawa, Proceedings of the 8th International Conference on the Chemistry of Cement, Rio de Janeiro, 1986, pp. 251–256.
[52] T. Sagawa, T. Ishida, Y. Yuan, T. Nawa, Hydrate composition analysis and microstructure characteristics of Portland cement—blast furnace slag system, J. JSCE 66 Part E (2010) 311–324, (in Japanese).
[53] Y. Suda, Y. Tanaka, T. Saeki, Fundamental study on chemical composition and physical properties, J. JSCE 66 Part E (2010) 528–544, (in Japanese).
[54] W. Ma, D. Sample, R. Martin, P.W. Brown, Calorimetric study of cement blends containing fly ash, silica fume, and slag at elevated temperatures, Cem. Concr. Agg. 16 (1994) 93–99.
[55] V. Rahhal, O. Cabrera, R. Talero, A. Delgado, Calorimetry of Portland cement with silica fume and gypsum additions, J. Therm. Anal. Calorim. 87 (2007) 331–336.
[56] A.K. Schindler, K.J. Folliard, Heat of hydration models for cementitious materials, ACI Mater. J. 102 (2005) 24–33.
[57] P.W. Brown, C.L. Hanner, E.J. Prosen, The effect of inorganic salts on tricalcium silicate hydration, Cem. Concr. Res. 16 (1985) 17–22.